



Article

Construction of a Predictive Model for Dynamic and Static Recrystallization Kinetics of Cast TC21 Titanium Alloy

Ziliang Li ^{1,2}, Yunpeng Chai ^{3,*} , Ling Qin ⁴ , Yanchun Zhu ³, Yong Niu ³, Jiaxin Fan ³ and Zhenwei Yue ³

¹ School of Electronic Information Engineering, Taiyuan University of Science and Technology, Taiyuan 030024, China; liziliang@tyust.edu.cn

² College of Mechanical and Vehicle Engineering, Taiyuan University of Technology, Taiyuan 030024, China

³ School of Mechanical Engineering, Taiyuan University of Science and Technology, Taiyuan 030024, China; 2013046@tyust.edu.cn (Y.Z.); 2019005@tyust.edu.cn (Y.N.); s202112210567@stu.tyust.edu.cn (J.F.); s202112210547@stu.tyust.edu.cn (Z.Y.)

⁴ Center of Innovation for Flow Through Porous Media, Department of Petroleum Engineering, University of Wyoming, Laramie, WY 82071, USA; lqin1@uwyo.edu

* Correspondence: s202212210073@stu.tyust.edu.cn

Abstract: In this study, hot compression experiments were conducted on cast TC21 titanium alloy using a Gleeble-1500D thermal simulation compression tester, and the hot-compressed specimens were heat-treated. The data obtained after analyzing the thermal compression of cast TC21 titanium alloy were analyzed to construct a thermal machining diagram with a strain of 0.8 and to optimize the machining window. This study investigated the microstructure of the alloy after hot pressing experiments and heat treatment, applying the study of the microstructure evolution law of cast TC21 titanium alloy. The analysis of the tissue evolution law established the dynamic and static recrystallization volume fraction as a function of heat deformation parameters. The results show that the optimal processing window for cast TC21 titanium alloy is a deformation temperature in the range of 1373 K–1423 K and a strain rate of 0.1 s^{-1} . The increase in deformation volume and deformation temperature both favor recrystallization and make the recrystallization volume fraction increase, but the increase in strain rate will inhibit the increase in the recrystallization degree to some extent. The dynamic and static recrystallization equations for the cast TC21 titanium alloy at different temperatures were constructed. The experimental measurements of recrystallization volume fraction are in good agreement with the predicted values.

Keywords: cast TC21 titanium alloy; thermal compression; thermal processing diagram; dynamic and static recrystallization; kinetic prediction model



Citation: Li, Z.; Chai, Y.; Qin, L.; Zhu, Y.; Niu, Y.; Fan, J.; Yue, Z.

Construction of a Predictive Model for Dynamic and Static Recrystallization Kinetics of Cast TC21 Titanium Alloy.

Crystals **2024**, *14*, 424. [https://](https://doi.org/10.3390/cryst14050424)

doi.org/10.3390/cryst14050424

Academic Editor: Petros Koutsoukos

Received: 18 April 2024

Revised: 28 April 2024

Accepted: 28 April 2024

Published: 29 April 2024



Copyright: © 2024 by the authors. Licensee MDPI, Basel, Switzerland. This article is an open access article distributed under the terms and conditions of the Creative Commons Attribution (CC BY) license (<https://creativecommons.org/licenses/by/4.0/>).

1. Introduction

Ti-6Al-2Sn-2Zr-3Mo-1Cr-1Nb (TC21) titanium alloy is an $\alpha + \beta$ damage tolerant titanium alloy with excellent fracture toughness, high specific strength, good plasticity, high corrosion resistance and excellent fatigue and creep properties [1,2]. Therefore, TC21 titanium alloy is widely used in manufacturing aircraft structures, engines and critical components of aerospace equipment, making it a high-quality material choice in these fields [3,4]. During the thermoplastic processing of metallic materials, the dual effect of temperature and deformation causes significant changes in the microstructure of the material, and these microstructure changes are manifested in macroscopic changes in material properties. When cast TC21 titanium alloy is present in the process of thermal deformation, in which the increase in the deformation process's hardening effect dominates, which leads to the rise of flow stress, dynamic recrystallization (DRX) phenomenon appears. When the flow stress reaches the peak, there will be a small drop; dynamic softening occurs when the DRX phenomenon dominates, and DRX can effectively improve metal plasticity and eliminate internal defects in the material [5]. Static recrystallization (SRX) occurs

in the heat treatment process between and after thermal deformation, and SRX can also effectively improve material plasticity to reduce the deformation resistance in the next step [6,7]. Therefore, the microstructure evolution of metal engineering materials in the thermoplastic processing stage has received a lot of attention from scholars and researchers. Liu et al. [8] studied the gradient deformation behavior, DRX kinetics and the microstructure evolution of nickel-based powdered high-temperature alloys by means of thermal gradient compression. The DRX kinetics of this high temperature alloy was established. Cano-Castillo et al. [9] investigated the effect of Ca or Nd on the microstructure and weave modification during indirect extrusion and after subsequent annealing of Mg-Zn-based alloys. It was found that the addition of these elements affected the recrystallization process and resulted in samples extruded at different extrusion speeds with significant weave changes. Cho et al. [10] proposed a historically relevant and physically driven internal state variable intrinsic model that simultaneously explains the effects of SRX, DRX and grain size on the mechanical behavior at different strain rates, temperatures and pressures. Brown et al. [11] proposed a new model to explain the evolution and softening behavior of material recrystallization, and the new model represents the internal state variables of dislocation density and spacing between geometrically necessary subgrain boundaries. Després et al. [12] found a primitive method to predict the development of SRX weaving during annealing of deformed crystalline materials with a model capable of input parameters measured directly on the orientation map of the deformed microstructure measured with electron backscatter diffraction. Luan et al. [13] developed a validated numerical model using the Kobayashi, Warren and Carter phase field model combined with crystal plasticity finite elements that predicts the incubation time of recrystallized grain structure, grain nucleation and weave evolution.

This study was conducted in order to characterize the material recrystallization volume fraction quantitatively during the thermal processing of the material, to achieve the prediction of the deformation of the fully recrystallized titanium alloy ingot, and to provide guidance and help for the development of the open billet forging process of cast TC21 titanium alloy. In this study, the specimens of cast TC21 titanium alloy were subjected to heat treatment experiments after hot compression experiments; the DRX volume fraction of cast TC21 titanium alloy was counted with the help of metallography, and the influence of deformation parameters on the microstructure after heat treatment was quantitatively analyzed to establish a dynamic and static recrystallization kinetic prediction model.

2. Experimental Materials and Procedure

2.1. Experimental Materials

The raw material used for the experiments is the cast TC21 titanium alloy, and the chemical composition of the material is shown in Table 1. The continuous heating metallographic method was used to measure the cast TC21 titanium alloy $\alpha + \beta \rightarrow \beta$ phase transition point of 1223 ± 5 K. The original microstructure of the material used in this experiment is shown in Figure 1, from which it can be seen that the straight β grain boundary (a typical grain boundary characteristic of the cast organization) exists with a continuous α phase, and the needle-like α organization is distributed within the β grain.

Table 1. Chemical composition of TC21 titanium alloy (wt%).

Al	Sn	Zr	Mo	Cr	Nb	Si	Fe	C	N	O	H	Ti
6.23	2.06	2.14	2.85	1.57	1.94	0.77	0.028	0.007	0.007	0.11	0.001	Bal.

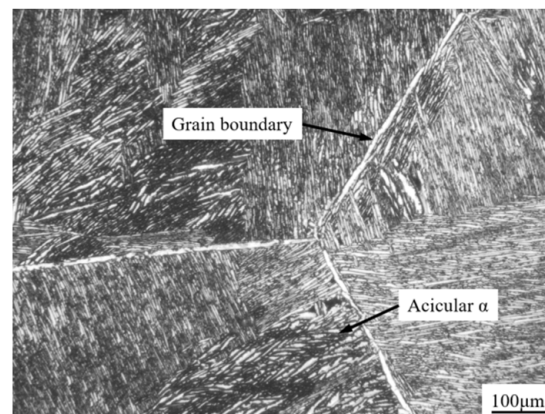


Figure 1. Original microstructure of TC21 titanium alloy in cast state.

2.2. Experimental Procedure

The specimens used in the thermal compression simulation experiment were cylinders with specifications of $\Phi 10 \text{ mm} \times 15 \text{ mm}$ obtained by wire cutting titanium alloy ingots with DK7735 taper type EDM wire cutting machine. The thermal simulation compression test was conducted on a Gleeble-1500D simulator, with tantalum pads at both ends of the specimen to ensure the flatness of the upper and lower ends of the specimen and to reduce the friction between the indenter and the specimen; the specimen was heated to the deformation temperature at a heating rate of 10 K/s, and the isothermal deformation was carried out after holding for 5 min. The specific experimental steps and samples before and after deformation are shown in Figure 2.

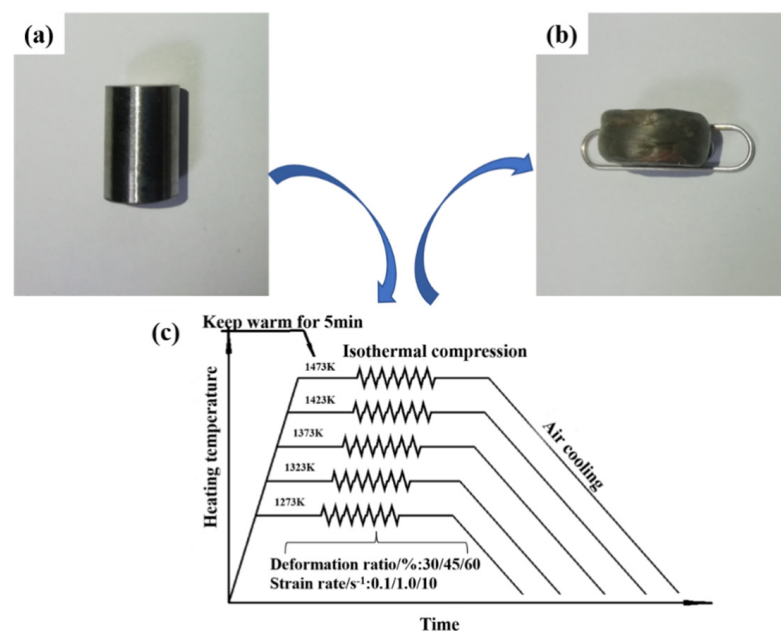


Figure 2. Before and after deformation of the sample and the flow chart of the experiment: (a) Sample before deformation; (b) Sample after deformation; (c) Experiment process.

The isothermal compressed specimens were heat treated and held at 1273 K for 30 min. After heat treatment, the specimens were quenched in water to preserve the microstructure of the material at high temperature. The heat-treated specimens were cut along the axial direction and underwent grinding, polishing and etching to produce the metallographic specimens required for the experiments.

3. Results and Discussion

3.1. Creation of a Thermal Processing Diagram

The use of thermal processing diagram can be more intuitive and offer clear understanding of the microstructure deformation mechanism of the material in the processing stage of stable areas and non-stable areas, such as cracking, to facilitate the optimization of the processing process; one can obtain a more ideal material organization and properties. The thermal processing diagram is a combination of a power dissipation diagram and an instability diagram overlapping in the deformation temperature and strain rate space, where the power dissipation diagram shows the tissue evolution of the material during the deformation phase, while the instability diagram can reveal the “safe zone” and “non-safe zone” of the material during the deformation phase. The combination of the two can clearly characterize the influence of the processing parameters on the high temperature plastic deformation phase of the material. Prasad et al. [14] reveal the process of material microstructure evolution with the energy dissipation rate, which is calculated as follows:

$$\eta = \frac{2m}{m+1} \quad (1)$$

where m is the strain rate sensitivity exponent.

The power dissipation rate is not the only factor to evaluate the superiority of the material processing performance, but it also needs to be closely related to the high temperature plastic deformation of the material. The instability diagram of a material is the parameter that judges the possibility of material instability of a metallic material during the thermal processing stage. A thermal processing diagram of the material can show the destabilization and safety regions of the material during thermal processing to optimize the processing and is also very important for the selection of optimal thermal processing parameters. The instability diagram is established by Prasad on the basis of the continuous instability criterion of the irreversible thermodynamic extremum principle, and its criterion instability formula can be the following:

$$\xi(\dot{\epsilon}) = \frac{\partial \ln(\frac{m}{1+m})}{\partial \ln \dot{\epsilon}} + m < 0 \quad (2)$$

When $\xi(\dot{\epsilon})$ is negative, it indicates that material destabilization occurs during deformation, but determining the exact form of destabilization requires a determination based on the specific microstructure.

In this study, the data of cast TC21 titanium alloy at the strain of 0.8 were used to calculate a thermal processing diagram with a deformation temperature range of 1273 K to 1473 K and a deformation rate range of 0.1 s^{-1} to 10 s^{-1} . The relevant data can be obtained according to the calculation formula of the strain rate sensitivity exponent m for cast TC21 titanium alloy, as shown in Table 2.

Table 2. Strain rate sensitivity exponent m values under different deformation conditions.

m $\ln \dot{\epsilon}$	Temperature/K				
	1273	1323	1373	1423	1473
−2.303	0.31076	0.25944	0.29648	0.32165	0.25585
0	0.17395	0.16166	0.16064	0.16263	0.14396
2.303	0.03715	0.06388	0.02480	0.00361	0.03207

The power dissipation diagram of cast TC21 titanium alloy at a strain of 0.8 is shown in Figure 3a. From the figure, it can be seen that the power dissipation rate increases gradually with decreasing strain rate. The values of the power dissipation rate are maximized in the region of 1273 K/ 0.01 s^{-1} and 1423 K/ 0.01 s^{-1} . The lower strain rate allows sufficient time for the material to recrystallize, and the alloy has easier recrystallized grain nucleation and higher thermal conversion. At the deformation condition of 1423 K/ 10 s^{-1} , the power

dissipation rate of the material is the lowest. This indicates that the recrystallization behavior under this condition is not obvious and the thermal conversion efficiency is very low, which is not an ideal processing region. Figure 3b shows the plastic instability diagram of cast TC21 titanium alloy at strain 0.8. A thermal processing diagram can be obtained by superimposing the power dissipation diagram and the plastic instability diagram, and the shaded area indicates the instability region, as shown in Figure 3c. The greater the power dissipation rate within the safe zone, the more likely the material will undergo DRX. It can be concluded by combining the processing diagrams that the more excellent processing window for cast TC21 titanium alloy is a deformation temperature of 1373 K–1423 K and strain rate of 0.1 s^{-1} .

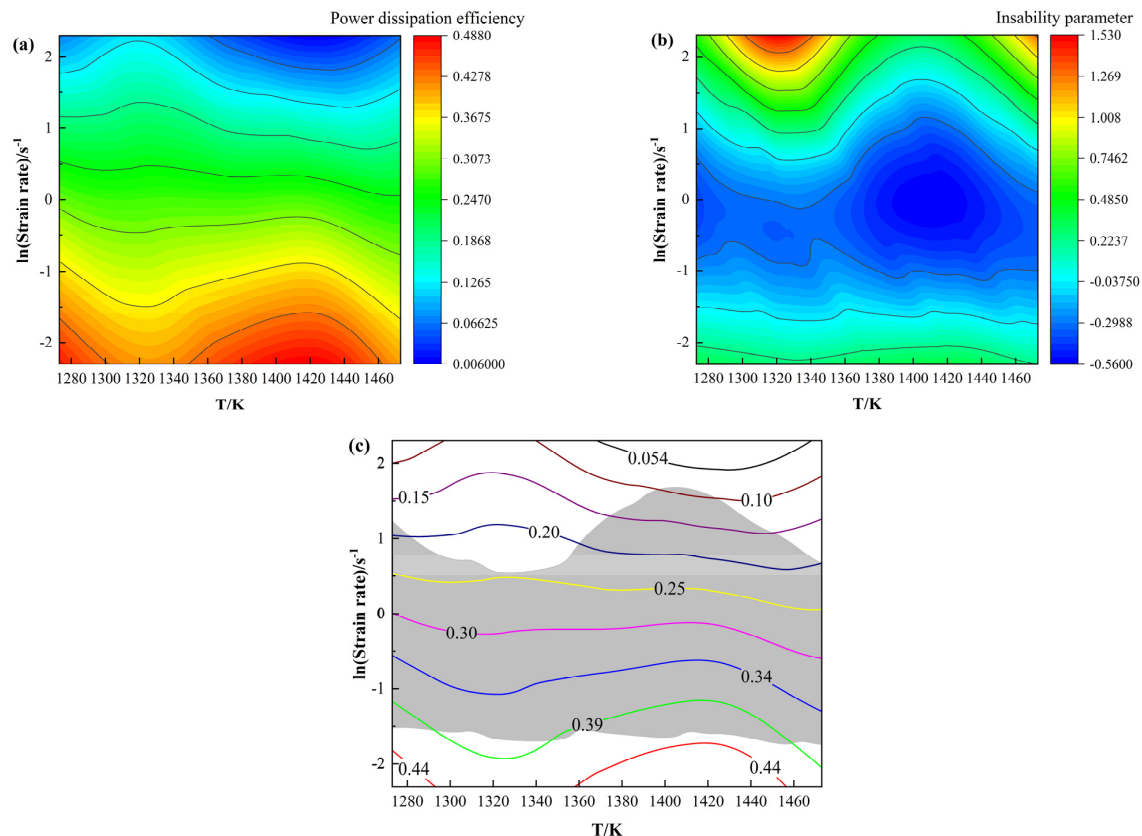


Figure 3. Cast TC21 titanium alloy at a strain of 0.8: (a) Energy dissipation diagram; (b) Plastic instability diagram; (c) Thermal processing diagram.

3.2. Microstructure Evolution

The microstructure of cast TC21 titanium alloy after hot compression under different deformation conditions is shown in Figure 4. From Figure 4a, it can be seen that, when the deformation amount is 30%, the grain boundary intersects with the original organization with obvious signs of widening and curving, and no recrystallized grains are seen at the grain boundary. With the increase of the deformation amount, when the deformation is 45% (as shown in Figure 4b), it can be clearly seen that the grain boundary morphology has changed significantly and DRX has appeared. When the deformation amount reaches 60%, a large number of fine recrystallized grains at the grain boundaries have already appeared. It shows that recrystallization can be induced to occur by an increase in the amount of deformation during thermal deformation. The main reason for this is that, as the deformation proceeds, a large amount of deformation energy accumulates within the material, causing a large number of recrystallized grains to appear at the grain boundaries. It can be seen that the increase in the degree of deformation can provide the driving force for DRX. Kong et al. [15] also found that increasing the amount of deformation promotes

DRX of Mg-Zn-Nd-Zr alloys. At low strain rates (0.1 s^{-1}), there are small, recrystallized grains at the grain boundaries (as shown in Figure 4c). When the strain rate increases to 1.0 s^{-1} or even 10 s^{-1} , the number of recrystallized grains at the grain boundaries increases, but the grain size does not increase significantly. When deformed at low temperature (1273 K), the grain boundaries are flat, and no recrystallized grains are seen at the grain boundaries. As the temperature increases, when the temperature reaches 1323 K, the grain boundaries become curved, and many recrystallized grains of different sizes can be seen at the grain boundaries (as shown in Figure 4c). The number of recrystallized grains at the grain boundaries increases significantly when the temperature increases to 1473 K. This shows that the increase in temperature can effectively promote the occurrence of DRX and the growth of grain size. As a result of the plastic deformation of the material at higher temperatures, the diffusion of atoms within the material is allowed to occur more easily, and the driving force for dislocation slip is higher, which can effectively promote the occurrence of DRX. Liu et al. [16] also found that the deformation temperature has a significant effect on grain size and grain size distribution.

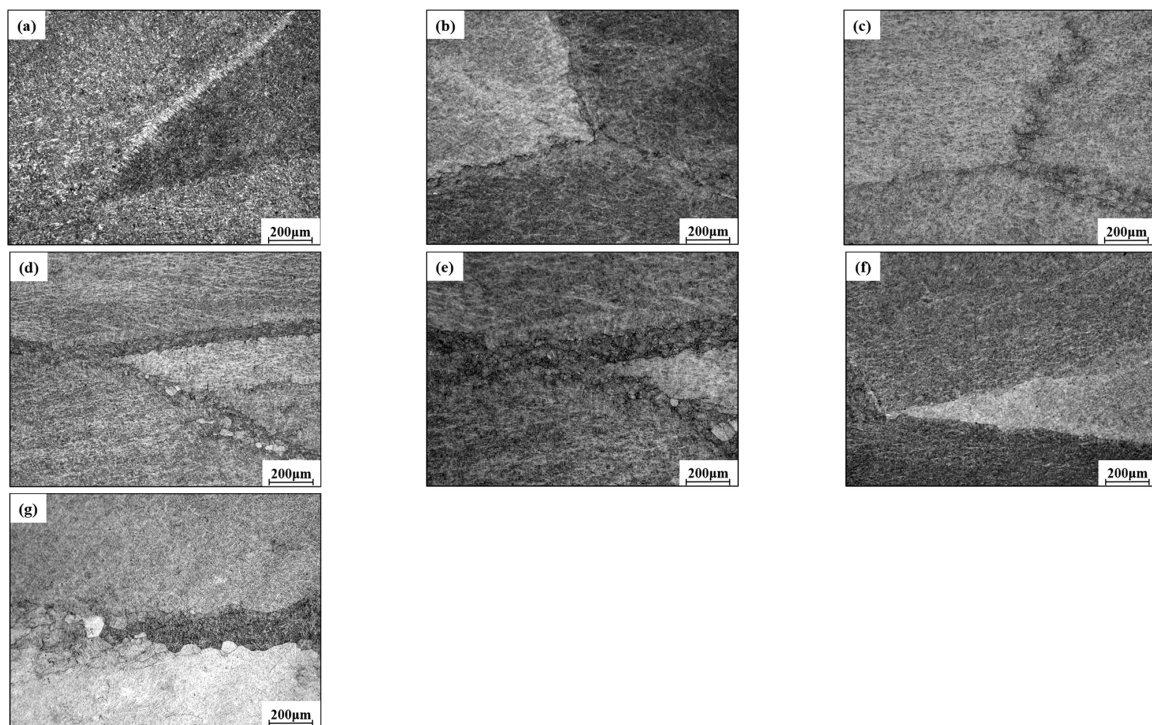


Figure 4. Microstructure of cast TC21 titanium alloy specimens under different deformation conditions: (a) $T = 1323 \text{ K}$, $\dot{\epsilon} = 0.1 \text{ s}^{-1}$, $R = 30\%$; (b) $T = 1323 \text{ K}$, $\dot{\epsilon} = 0.1 \text{ s}^{-1}$, $R = 45\%$; (c) $T = 1323 \text{ K}$, $\dot{\epsilon} = 0.1 \text{ s}^{-1}$, $R = 60\%$; (d) $T = 1323 \text{ K}$, $\dot{\epsilon} = 1.0 \text{ s}^{-1}$, $R = 60\%$; (e) $T = 1323 \text{ K}$, $\dot{\epsilon} = 10 \text{ s}^{-1}$, $R = 60\%$; (f) $T = 1273 \text{ K}$, $\dot{\epsilon} = 0.1 \text{ s}^{-1}$, $R = 60\%$; (g) $T = 1473 \text{ K}$, $\dot{\epsilon} = 0.1 \text{ s}^{-1}$, $R = 60\%$.

Through the above analysis, it can be understood that the deformation volume, strain rate and deformation temperature have more or less influence on the occurrence of DRX during the deformation of cast TC21 titanium alloy. The influence of deformation volume and deformation temperature on the DRX of its titanium alloy is significantly greater than the influence of strain rate on its degree.

Figure 5 shows the microstructure photographs of cast TC21 titanium alloy after hot compression and heat treatment under different deformation conditions. It can be seen from Figure 5a that, when the deformation reaches 30%, recrystallized grains with relatively large length and width are precipitated at the grain boundaries along the 45° direction. This direction is more prone to cracking during the deformation of the alloy and stores more deformation energy, which effectively promotes the occurrence of recrystallization.

Lu et al. [17] studied the DRX behavior of Ti-25V-15Cr-0.2Si alloy and found that the recrystallized grains formed a “necklace” structure along the grain boundaries. When the deformation amount reaches 45%, it can be clearly seen that the recrystallized grains tend to be equiaxed and the degree of recrystallization is better than under small deformation amount (30%), as shown in Figure 5b. The increase in the amount of deformation up to 60% continues to increase the degree of recrystallization, and the grain size continues to grow, as shown in Figure 5c. This shows that the amount of deformation has a significant effect on the recrystallization after heat treatment, and the large deformation will give more driving force to the recrystallized grains after heat treatment to make them grow further. As can be seen by comparing Figure 5a,d, the cast TC21 titanium alloy deformed at a relatively high temperature (1373 K), and a heat-treated condition results in larger recrystallized grain size and better isometricity as compared to the low temperature (1273 K) condition. With the continued increase in temperature, the recrystallized grains continue to grow, and individual grains are oversized and significantly coarsened when the temperature reaches 1473 K, as shown in Figure 5e. It suggests that too high a deformation temperature after heat treatment is detrimental to the refinement of the organization of the cast alloy. Zhu et al. [18] investigated the recrystallization behavior of cast Ti-25V-15Cr-0.3Si titanium alloy and found that an increase in temperature resulted in a significant increase in the size of recrystallized grains. It can be seen from Figure 5f that the size of the recrystallized grains precipitated at the grain boundaries increases significantly when the strain rate is 1 s^{-1} , which is not homogeneous in size and remains in an unstable state with a tendency to continue to grow. When the strain rate increases to 10 s^{-1} , the grain boundary of the grain becomes rounded and has a good isometric degree, but the grain size does not grow significantly, as shown in Figure 5g. The main reason for this is that an increase in strain rate effectively increases the distortion energy while hindering the nucleation of recrystallized grains. Therefore, the increase in strain rate is not conducive to recrystallization to a certain extent.

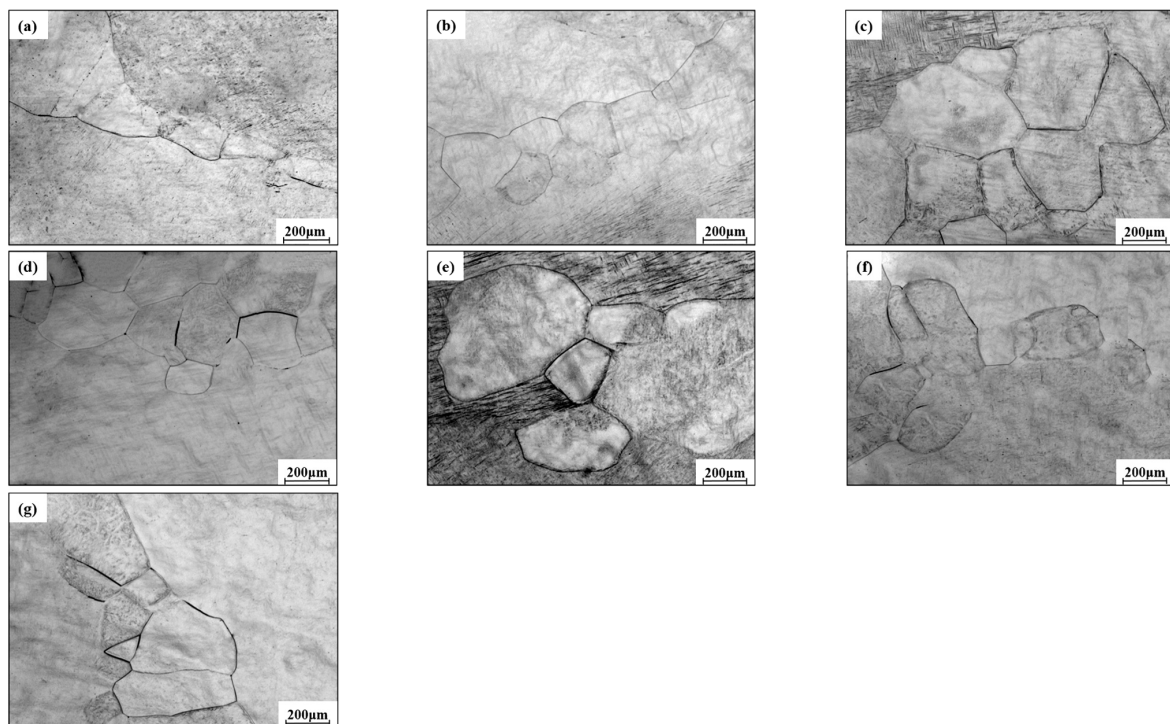


Figure 5. Microstructure of cast TC21 titanium alloy under different deformation conditions after heat treatment: (a) $T = 1273 \text{ K}$, $\dot{\epsilon} = 0.1 \text{ s}^{-1}$, $R = 30\%$; (b) $T = 1273 \text{ K}$, $\dot{\epsilon} = 0.1 \text{ s}^{-1}$, $R = 45\%$; (c) $T = 1273 \text{ K}$, $\dot{\epsilon} = 0.1 \text{ s}^{-1}$, $R = 60\%$; (d) $T = 1373 \text{ K}$, $\dot{\epsilon} = 0.1 \text{ s}^{-1}$, $R = 30\%$; (e) $T = 1473 \text{ K}$, $\dot{\epsilon} = 0.1 \text{ s}^{-1}$, $R = 30\%$; (f) $T = 1273 \text{ K}$, $\dot{\epsilon} = 1 \text{ s}^{-1}$, $R = 30\%$; (g) $T = 1273 \text{ K}$, $\dot{\epsilon} = 10 \text{ s}^{-1}$, $R = 30\%$.

3.3. Determination of Recrystallization Volume Fraction

During thermal deformation, the internal organization of the material directly affects the mechanical properties of the products it manufactures, and because the stresses on the material are not uniform during compression, this leads to different deformation zones in the cross section, mainly difficult, small and large deformation zones [19], as shown in Figure 6. The large deformation zone experiences the greatest stress under the combined action of high temperature and external forces, resulting in significant recrystallization phenomena, while the small and difficult deformation zones experience lower stress and a lower degree of recrystallization. The deformation in the core of the specimen is uniform; the organizational state is representative, and it can accurately reflect the overall performance of the material. In order to investigate the dynamic and static recrystallization of cast TC21 titanium alloy after heat treatment, the tissue photographs of the core of the specimen were used as the object of dynamic and static recrystallization statistics. The alloy recrystallization was quantitatively analyzed with the help of image-processing software Adobe Photoshop CS (PS) and image analysis software Image-Pro Plus6.0 (IPP6.0) for the subsequent establishment of dynamic and static recrystallization, which provided reliable and detailed data support for the establishment of dynamic and static recrystallization kinetics.

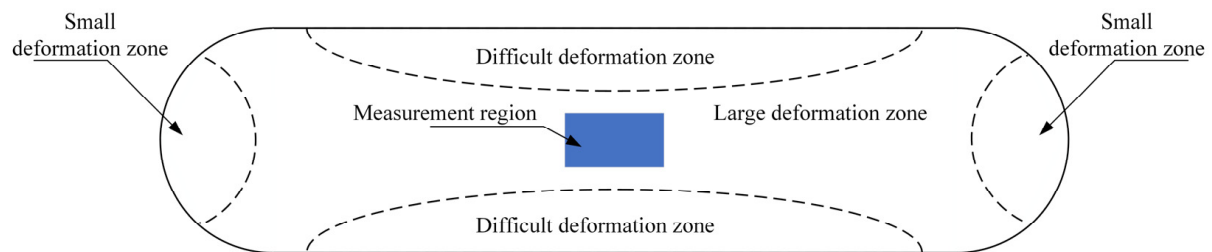


Figure 6. Schematic diagram of the deformation area of the specimen and the location of the metallographic photograph.

To accurately determine the recrystallization volume fraction of cast TC21 titanium alloy, Figure 7a was converted into a black and white image using the image processing software PS to enhance the grains and grain boundaries, and, then, the processed image was imported into the image analysis software IPP6.0 to set the scale and select parameters (such as aspect ratio, area and size). The grains were numbered (as shown in Figure 7c). Finally, each grain-specific parameter was exported as a text file, which was used to calculate the aspect ratio, area and dimensions of each heat-treated grain based on the area measurement method ($X_{RX} = \sum Area(\beta_{RX}) / \sum Area_{total}$) to derive the recrystallization volume fraction.

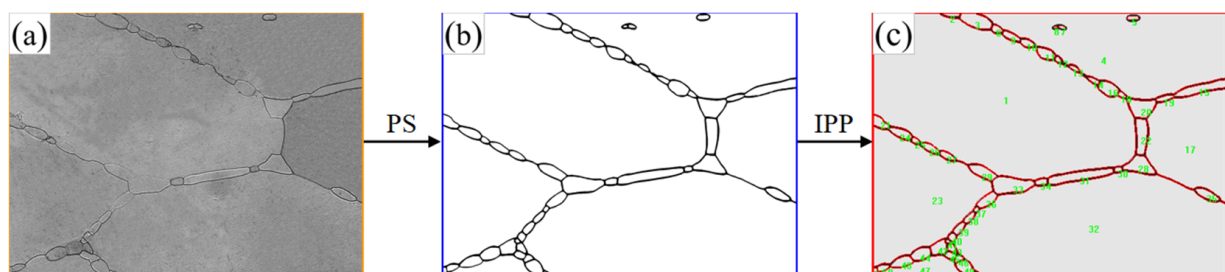


Figure 7. Image processing and recrystallization volume fraction calculation process: (a) Original image; (b) Processed image; (c) Grain statistics.

Figure 8 shows the recrystallization volume fraction of cast TC21 titanium alloy after hot compression and heat treatment. Comparing the recrystallization volume fraction under different strain rate conditions, it is found that the volume fraction increases with the increase of deformation and temperature, which indicates that the increase of temperature provides more energy for the slip and climb of dislocations, which moves faster, and recrystallization occurs more easily [20]. The increase in deformation can increase the internal distortion energy of the material and provide the driving force for recrystallization to occur. In comparison, it is found that Figure 8a to Figure 8c can clearly show that the DRX volume fraction decreases slightly with increasing strain rate, which is mainly because strain rates that are too high lead to too fast deformation of the specimens and a short time for recrystallization to occur before nucleation [21]. Therefore, a too high strain rate is detrimental to the increase in the recrystallization volume fraction.

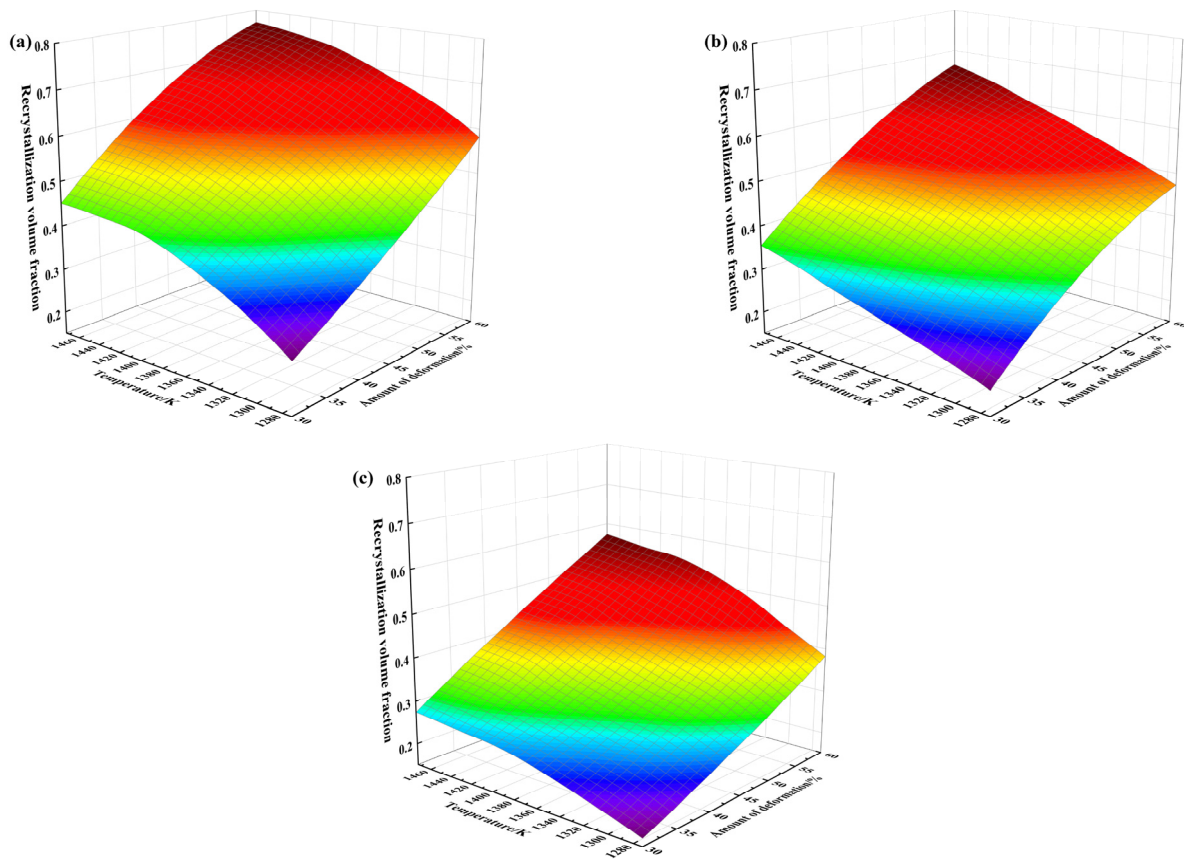


Figure 8. Volume fraction of recrystallization of the specimen after thermal deformation and heat treatment: (a) $\dot{\epsilon} = 0.1 \text{ s}^{-1}$; (b) $\dot{\epsilon} = 1.0 \text{ s}^{-1}$; (c) $\dot{\epsilon} = 10 \text{ s}^{-1}$.

3.4. Construction of Recrystallization Kinetic Equation

According to the basic characteristics of the kinetics of recrystallization nucleation and growth, the present study is mainly based on the kinetic equations described by the Johnson–Mehl–Avrami–Kolmogorov (JMAK) model [22,23]:

$$X = 1 - \exp \left[-\beta \left(A \epsilon^a Z^{-b} \right)^k \right] \quad (3)$$

where β is the coefficient related to the deformation parameter, A is the kinetic constant, ϵ is the strain, a is a coefficient related to the strain, b is the coefficient related to the strain rate and deformation temperature, k is the recrystallization index and Z is the Zener–Hollomon factor.

The A , β , a , b and k are the fitted data in the curve obtained after fitting. At a certain deformation temperature, the dynamic and static recrystallization of the specimen core can be considered to be related to the deformation amount and the strain rate [24,25]. Therefore, based on the extracted volume fractions of dynamic and static recrystallization under different deformation conditions, the kinetic equation of dynamic and static recrystallization under different deformation temperatures was derived by combining with Equation (3):

$$X = \begin{cases} 1 - \exp\left(-0.7228\epsilon^{1.0744}\dot{\epsilon}^{-0.1459}\right) & (T = 1273 \text{ K}) \\ 1 - \exp\left(-1.0184\epsilon^{1.0501}\dot{\epsilon}^{-0.1130}\right) & (T = 1373 \text{ K}) \\ 1 - \exp\left(-1.2802\epsilon^{1.0746}\dot{\epsilon}^{-0.1338}\right) & (T = 1473 \text{ K}) \end{cases} \quad (4)$$

In order to get a more objective and clear understanding of the agreement between the calculated and experimental values of the dynamic and static recrystallization volume fractions, the experimental values of dynamic and static recrystallization volume fractions were compared with the calculated values, and the comparison results are shown in Table 3. The correlation between the experimental values and the calculated values of the prediction model constructed in this study was derived by linearly fitting the experimental values to the calculated values, as shown in Figure 9. It is obvious from Table 3 that the experimentally measured values of recrystallization volume fraction under each condition do not differ much from the computed values. The maximum absolute error value of 3.4% occurs at a deformation temperature of 1273 K and a strain of 0.6. The minimum error of 2.0% occurs at a temperature of 1273 K and a strain of 0.9. The correlation coefficient between the experimental value of dynamic and static recrystallization volume fraction and the calculated value of the model is $R^2 = 0.97993$. In the comprehensive analysis, the prediction model constructed in this study can describe the recrystallization behavior of the casting TC21 titanium alloy in the process of heat deformation to a certain extent.

Table 3. Comparison of experimentally measured and computed values of dynamic and static recrystallization volume fraction at a strain rate of 1 s^{-1} .

Temperature/K	Experimental Measurement Values			Computed Values		
	Strain 0.36	Strain 0.6	Strain 0.9	Strain 0.36	Strain 0.6	Strain 0.9
1273	20.3%	37.5%	47.3%	21.4%	34.1%	47.5%
1373	28.3%	47.8%	57.9%	29.4%	44.8%	59.8%
1473	35.4%	54.2%	66.6%	37.4%	52.5%	68.1%

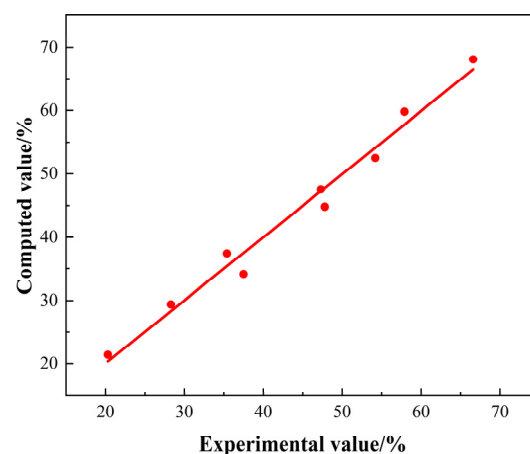


Figure 9. Correlation between experimental and computed values of dynamic and static recrystallization volume fraction of cast TC21 alloy.

4. Conclusions

In this paper, the processing window is optimized based on hot compression experiments, and a prediction model of dynamic and static recrystallization of cast TC21 titanium alloy is constructed based on the effects of different deformation parameters on the dynamic and static recrystallization of cast TC21 titanium alloy during hot compression experiments and heat treatment experiments. The main results of the study are as follows:

- (1) The thermal processing diagram of cast TC21 titanium alloy at a strain of 0.8 was constructed, and a more ideal processing window was obtained by combining the power dissipation diagram and plastic instability diagram—deformation temperature of 1373 K–1423 K and strain rate of 0.1 s^{-1} .
- (2) The microstructure of cast TC21 titanium alloy was observed and analyzed with hot compression tests and heat treatment tests, and it was found that the deformation amount, deformation temperature and strain rate had different effects on the recrystallization of cast TC21. The increase in deformation volume and deformation temperature can provide more energy for DRX, which is beneficial to the nucleation and growth of recrystallized grains, while the increase in strain rate suppresses the nucleation rate of recrystallization to a certain extent.
- (3) The dynamic and static recrystallization volume fractions of cast TC21 titanium alloy after heat treatment were extracted, and the fitted dynamic and static recrystallization volume fractions were plotted. It is found that the dynamic and static recrystallization volume fraction increases with decreasing strain rate and increasing deformation temperature.
- (4) According to the existing recrystallization kinetic equations, combined with the experimental situation of casting TC21 titanium alloy, the dynamic and static recrystallization kinetic models of cast TC21 titanium alloy under different deformation temperatures were established:

$$X = \begin{cases} 1 - \exp\left(-0.7228\epsilon^{1.0744}\dot{\epsilon}^{-0.1459}\right) & (T = 1273 \text{ K}) \\ 1 - \exp\left(-1.0184\epsilon^{1.0501}\dot{\epsilon}^{-0.1130}\right) & (T = 1373 \text{ K}) \\ 1 - \exp\left(-1.2802\epsilon^{1.0746}\dot{\epsilon}^{-0.1338}\right) & (T = 1473 \text{ K}) \end{cases}$$

Author Contributions: Conceptualization, Y.Z.; validation, Z.Y.; formal analysis, Y.C. and L.Q.; investigation, Z.L.; data curation, Z.L., Y.C., L.Q., J.F. and Z.Y.; writing—original draft preparation, Z.L. and Y.Z.; writing—review and editing, Y.C., L.Q., Y.N. and J.F.; funding acquisition, Y.Z. and Y.N. All authors have read and agreed to the published version of the manuscript.

Funding: This work was supported by the National Natural Science Foundation of China (No. 52375363), the Applied Basic Research Project of Shanxi Province (No. 202203021211208) and (No. 20210302123203), Technological Innovation Talent Team Special Plan of Shanxi Province (202204051002002).

Data Availability Statement: Data are contained within the article.

Conflicts of Interest: The authors declare no conflict of interest.

References

1. Yuan, B.; Zheng, Y.; Wang, Y.; Chen, Q.; Gong, L.; Lv, M. Effect of temperature on hydrogen absorption characteristic and microstructural evolution of TC21 alloy. *J. Alloys Compd.* **2015**, *648*, 794–802. [\[CrossRef\]](#)
2. Zhu, Y.; Zeng, W.; Sun, Y.; Feng, F.; Zhou, Y. Artificial neural network approach to predict the flow stress in the isothermal compression of as-cast TC21 titanium alloy. *Comp. Mater. Sci.* **2011**, *50*, 1785–1790. [\[CrossRef\]](#)
3. Li, X.; Ouyang, D.; Zhang, K.; Wang, K.; Cui, K. Hot deformation characteristic of TC21 titanium alloy with lamellar microstructure. *Mater. Today Commun.* **2024**, *39*, 108709. [\[CrossRef\]](#)
4. Wang, Y.; Yang, G.; Zhang, S.; Xiu, S. Effect of crystal orientation on micro-stress distribution in a damage-tolerant titanium alloy TC21. *J. Alloys Compd.* **2022**, *924*, 166637. [\[CrossRef\]](#)
5. Wang, B.; Zhao, H.; Shan, X.; Tang, Y.; Wang, B.; Tian, Y. Hot deformation behavior and dynamic recrystallization mechanism of $\text{Ti}_2\text{ZrTa}_{0.75}$ refractory complex concentrated alloy. *Mater. Charact.* **2023**, *203*, 113061. [\[CrossRef\]](#)

6. Hu, Y.; Li, Y.; Zhang, S.; Lin, X.; Wang, Z.; Huang, W. Effect of solution temperature on static recrystallization and ductility of Inconel 625 superalloy fabricated by directed energy deposition. *Mater. Sci. Eng. A* **2020**, *772*, 138711. [\[CrossRef\]](#)
7. Zhang, L.; Wu, X.; Yang, X.; Li, Y. Static recrystallization and precipitation behavior of forged and annealed Mg-8.7Gd-4.18Y-0.42Zr magnesium alloy. *Mater. Today Commun.* **2023**, *34*, 105106. [\[CrossRef\]](#)
8. Liu, Y.; Liu, Z.; Wang, M. Gradient microstructure evolution under thermo-mechanical coupling effects for a nickel-based powder metallurgy superalloy—Dynamic recrystallization coexist with static recrystallization. *J. Mater. Process. Technol.* **2021**, *294*, 117142. [\[CrossRef\]](#)
9. Cano-Castillo, G.; Victoria-Hernández, J.; Bohlen, J.; Letzig, D.; Kainer, K. Effect of Ca and Nd on the microstructural development during dynamic and static recrystallization of indirectly extruded Mg–Zn based alloys. *Mater. Sci. Eng. A* **2020**, *793*, 139527. [\[CrossRef\]](#)
10. Cho, H.; Hammi, Y.; Bowman, A.; Karato, S.; Baumgardner, J.; Horstemeyer, M. A unified static and dynamic recrystallization Internal State Variable (ISV) constitutive model coupled with grain size evolution for metals and mineral aggregates. *Int. J. Plasticity* **2019**, *112*, 123–157. [\[CrossRef\]](#)
11. Arthur, A.; Douglas, J. Validation of a model for static and dynamic recrystallization in metals. *Int. J. Plast.* **2012**, *32–33*, 17–35.
12. Després, A.; Mithieux, J.; Sinclair, C. Modelling the relationship between deformed microstructures and static recrystallization textures: Application to ferritic stainless steels. *Acta Mater.* **2021**, *219*, 117226. [\[CrossRef\]](#)
13. Luan, Q.; Lee, J.; Zheng, J.; Hopper, C.; Jiang, J. Combining microstructural characterization with crystal plasticity and phase-field modelling for the study of static recrystallization in pure aluminium. *Comp. Mater. Sci.* **2020**, *173*, 109419. [\[CrossRef\]](#)
14. Prasad, Y.; Gegel, H.; Doraivelu, S.; Malas, J.; Morgan, J.; Lark, K.; Barker, D. Modeling of dynamic material behavior in hot deformation: Forging of Ti-6242. *Metall. Trans. A* **1984**, *15*, 1883–1892. [\[CrossRef\]](#)
15. Kong, F.; Yang, Y.; Chen, H.; Liu, H.; Fan, C.; Xie, W.; Wei, G. Dynamic recrystallization and deformation constitutive analysis of Mg–Zn–Nd–Zr alloys during hot rolling. *Heliyon* **2022**, *8*, e09995. [\[CrossRef\]](#) [\[PubMed\]](#)
16. Liu, Y.; Yao, Z.; Ning, Y.; Nan, Y. Effect of deformation temperature and strain rate on dynamic recrystallized grain size of a powder metallurgical nickel-based superalloy. *J. Alloys Compd.* **2017**, *691*, 554–563. [\[CrossRef\]](#)
17. Lu, S.; Ouyang, D.; Cui, X.; Wang, K. Dynamic recrystallization behavior of burn resistant titanium alloy Ti–25V–15Cr–0.2Si. *Trans. Nonferrous Met. Soc.* **2016**, *26*, 1003–1010. [\[CrossRef\]](#)
18. Zhu, Y.; Huang, Q.; Shi, X.; Shuai, M.; Zeng, W.; Zhao, Y.; Huang, Z.; Ma, L. Precipitation location of secondary phase and microstructural evolution during static recrystallization of as-cast Ti–25V–15Cr–0.3Si titanium alloy. *Trans. Nonferrous Met. Soc.* **2018**, *28*, 1521–1529. [\[CrossRef\]](#)
19. Wan, P.; Kang, T.; Li, F.; Gao, P.; Zhang, L.; Zhao, Z. Dynamic recrystallization behavior and microstructure evolution of low-density high-strength Fe–Mn–Al–C steel. *J. Mater. Res. Technol.* **2021**, *15*, 1059–1068. [\[CrossRef\]](#)
20. Zhang, W.; Yan, Z.; Wang, R.; Li, D.; Kang, Y.; Wu, Z.; Yang, X. Hot Deformation Behavior and Recrystallization Structure of Fe–1.3C–5Cr–0.4Mo–0.4V Ultra High Carbon Steel. *J. Mech. Eng.* **2020**, *56*, 116–123.
21. Matruprasad, R.; Ravi, R.; Surjya, K.; Shiv, B. EBSD study of microstructure evolution during axisymmetric hot compression of 304LN stainless steel. *Mater. Sci. Eng. A* **2018**, *711*, 378–388.
22. Fan, X.; Zhang, Y.; Zheng, H.; Zhang, Z.; Gao, P.; Zhan, M. Pre-processing related recrystallization behavior in β annealing of a near- β Ti–5Al–5Mo–5V–3Cr–1Zr titanium alloy. *Mater. Charact.* **2018**, *137*, 151–161. [\[CrossRef\]](#)
23. Xu, J.; Zeng, W.; Zhang, X.; Zhou, D. Analysis of globularization modeling and mechanisms of alpha/beta titanium alloy. *J. Alloys Compd.* **2019**, *788*, 110–117. [\[CrossRef\]](#)
24. Wang, H.; Qin, G.; Li, C.; Liang, G. Effect of deformation parameters and Al₂Cu evolution on dynamic recrystallization of 2219-O Al alloy during hot compression. *J. Mater. Res. Technol.* **2023**, *26*, 4093–4106. [\[CrossRef\]](#)
25. Che, B.; Lu, L.; Wu, Z.; Zhang, H.; Ma, M.; Luo, J.; Zhao, H. Dynamic recrystallization behavior and microstructure evolution of a new Mg–6Zn–1Gd–1Er alloy with and without pre-aging treatment. *Mater. Charact.* **2021**, *184*, 111506. [\[CrossRef\]](#)

Disclaimer/Publisher’s Note: The statements, opinions and data contained in all publications are solely those of the individual author(s) and contributor(s) and not of MDPI and/or the editor(s). MDPI and/or the editor(s) disclaim responsibility for any injury to people or property resulting from any ideas, methods, instructions or products referred to in the content.